Published in Surface Science 374, issues 1-3, 104-116, 1997
which should be used for any reference to this work


# Surface alloy formation and interdiffusion in $(\sqrt{5} \times \sqrt{5})R27°$–Yb/Al(001): a combined low-energy electron diffraction and X-ray photoelectron diffraction study

R. Fasel [a,*], M. Gierer [b], H. Bludau [b], P. Aebi [a], J. Osterwalder [c], L. Schlapbach [a]

[a] *Institut de Physique, Université de Fribourg, Pérolles, 1700 Fribourg, Switzerland*
[b] *Fritz-Haber-Institut der Max-Planck-Gesellschaft, Faradayweg 4–6, 14195 Berlin, Germany*
[c] *Physik-Institut, Universität Zürich-Irchel, Winterthurerstrasse 190, 8057 Zürich, Switzerland*

**Abstract**

We have investigated the atomic structure of $(\sqrt{5} \times \sqrt{5})R27°$–Yb/Al(001) by low-energy electron diffraction and angle-scanned full-hemispherical X-ray photoelectron diffraction. Quantitative agreement between the results from the two methods is obtained. We find that the Yb atoms occupy substitutional sites, thus removing every fifth surface Al atom. The residual first-layer Al atoms are displaced by more than 0.5 Å from their equilibrium position, in a way that results in a quasi-twelve-fold Al coordination for the Yb atoms. An expansion of the outermost substrate layer spacing and anomalously large vibrational amplitudes for the Al atoms of this strongly reconstructed first substrate layer are determined. Furthermore, a small fraction of Yb atoms is identified to occupy second-layer sites in otherwise unreconstructed surface patches. The comparison of the results obtained from the two techniques indicates the importance of a treatment of thermal vibrations going beyond the traditional Debye–Waller model in adsorbate X-ray photoelectron diffraction.

*Keywords:* Aluminum; Chemisorption; Low energy electron diffraction (LEED); Low index single crystal surfaces; Metal–metal interfaces; Photoelectron diffraction; Surface relaxation and reconstruction; Ytterbium

## 1. Introduction

The understanding of many surface properties is strongly based on a knowledge of the precise surface geometry. To date, the most prominent technique for the determination of surface structures has been low-energy electron diffraction (LEED) [1]. Another method for structure determination which has become more and more established in recent years is angle-scanned X-ray photoelectron diffraction (XPD) [2]. For some systems, good agreement between the results from LEED and XPD studies has been achieved [3,4], while for other systems the two methods yield contradictory results [5]. A combined, comparative study of a non-trivial surface structure may give insight into some of the reasons for this uncomfortable situation.

LEED and XPD are complementary methods in some aspects. LEED probes only that part of the surface which shows long-range order, whereas XPD is sensitive to the very local order around each individual photoemitter, even in the absence of long-range order. For the case of surface alloy formation or interdiffusion, XPD has been shown

*Corresponding author. Fax: +41 26 300 9747;
e-mail: roman.fasel@unifr.ch

to give very direct structure information [6], which in turn may be used as starting configuration for a LEED intensity analysis. Detailed structural information for the first few layers can then be obtained by LEED, whereas XPD is particularly sensitive to the structure above the photoemitter.

Initially, the study of the Yb/Al(001) system was motivated by the question whether an isolated Yb atom adsorbed on Al(001) is in the divalent $4f^{14}$, a mixed-valent $4f^{14-\delta}$ or the trivalent $4f^{13}$ state, and whether with increasing coverage a valence change occurs. The question of valency is strongly related to structural aspects: in the trivalent or mixed-valent state, the radius of the Yb atom is considerably decreased due to the less efficient screening of the core potential upon cracking of the 4f shell. The $YbAl_2$ and $YbAl_3$ bulk systems have been shown to be homogeneous mixed-valent [7], whereas surface-sensitive techniques indicated divalent Yb on the surface [8,9].

In this paper, we report on a combined LEED and XPD study of the $(\sqrt{5}\times\sqrt{5})$R26.6°–Yb/Al (001) surface structure ($\sqrt{5}$ structure) [10]. This structure is obtained either by room-temperature evaporation of 0.2 ML Yb on Al(001), or, alternatively by annealing of thicker Yb films. It therefore represents the most stable adsorption geometry for Yb/Al(001). We find that the Yb atoms occupy substitutional sites, thus removing every fifth surface Al atom. The Yb hard-sphere radius determined from the structural parameters is close to the bulk value for the metallic fcc structure, where Yb is divalent. This provides evidence that no valence change occurs upon condensation into the $\sqrt{5}$ structure. Furthermore, a small fraction of Yb atoms is identified to occupy second-layer sites in otherwise unreconstructed surface patches. It is shown that these subsurface Yb atoms are in a mixed valent $4f^{14-\delta}$ state.

## 2. Experiments and calculations

The XPD experiments were performed at the University of Fribourg in a VG ESCALAB Mark II spectrometer modified for motorized sequential angle-scanning data acquisition, and with a working pressure in the lower $10^{-11}$ mbar region. Photoelectron spectra and diffraction patterns were measured using Si K $\alpha$($h\nu = 1740$ eV) radiation, which allowed the excitation of the Yb 3d and Al ls core levels. All experiments were performed at room temperature. Contamination-free surfaces were prepared by a combination of $Ar^+$ sputtering and annealing at 500°C. Yb was evaporated from a resistively heated stainless-steel crucible onto the substrate. During Yb deposition, the pressure was in the lower $10^{-10}$ mbar range. The purity of the deposited Yb layers, as well as the coverage, was checked by core-level photoemission. The $(\sqrt{5}\times\sqrt{5})$R26.6°–Yb overlayers were obtained in two different ways. Either a nominal amount of 0.2 ML Yb was deposited on the Al(001) substrate which was kept at room temperature, or a thicker Yb film (>1 ML) was annealed to 400°C. For both ways of preparation, the LEED pattern of the Yb overlayers showed sharp overlayer spots and a low background, indicating a high degree of long-range order. Identical photoelectron spectra and photoelectron diffraction patterns were obtained for the samples prepared in the two different ways. To minimize the effects of accumulating contaminants, a fast data-acquisition mode was chosen for the full-hemispherical photoelectron diffraction experiments. For each of the 5044 angular settings, the total intensity was recorded at the kinetic energy corresponding to the maximum of the Yb $3d_{5/2}$ peak ($I_{peak}$) and at its high- and low-energy footpoints ($I_{high}$ and $I_{low}$, respectively). The background-corrected intensity was then calculated by subtracting the mean value of $I_{high}$ and $I_{low}$ from $I_{peak}$. It was verified that experiments using this fast mode of data acquisition gave identical results as using a more detailed but also more time-consuming mode, where the entire Yb $3d_{5/2}$ photoelectron spectrum is measured and integrated and a linear background subtracted.

Diffraction patterns were calculated using a single-scattering cluster (SSC) code as implemented by Friedman and Fadley [11], which includes spherical wave corrections [12]. The proper d initial state was taken into account for the calculations of the Yb $3d_{5/2}$ diffraction patterns. Radial matrix elements and phase shifts for p and f wave emission were calculated using a

computer code following the approach of Yeh and Lindau [13]. To judge the quality of the fit between calculation and experiment, a new $R$ factor ($R_{MP}$) was used [14]. This $R$ factor, which is based on the space of multipole expansion coefficients rather than emission angles, has been successfully used in previous quantitative XPD investigations [3–5].

The LEED experiments were performed in a separate UHV chamber (base pressure $7 \times 10^{-11}$ mbar), equipped with a display-type four-grid LEED optics and standard techniques for surface cleaning and characterization. Sample cleaning and preparation of Yb overlayers was performed as for the XPD experiments described above. The sample temperature was measured with a thermocouple which was spot-welded to the rear side of the crystal. LEED intensity measurements were performed at normal incidence of the primary beam at a sample temperature of 60 K. A computer-controlled video camera was used to record integrated spot intensities from the fluorescent screen. Normal incidence was adjusted using the $I$–$E$ curves of symmetry-equivalent beams. All $I$–$E$ curves were background corrected and normalized to a constant incidence beam current.

In the LEED program [15], nine phase shifts of Al and Yb were used which were calculated as described in Ref. [16]. The thermally induced vibrations of atoms were taken into account within the framework of the Debye–Waller approximation. The agreement between experimental and theoretical intensity data was quantified both by the $R_{DE}$ factor introduced by Kleinle et al. [17] and by Pendry's $R$ factor $R_P$ [18]. A non-linear least-squares optimization scheme allowing a simultaneous refinement of structural and non-structural parameters with respect to the $R_{DE}$ factor [19] and the $R_P$ factor [20] was applied.

## 3. Results and discussion

### 3.1. XPD measurements and structural analysis by LEED

The experimental Yb $3d_{5/2}$ XPD pattern from $(\sqrt{5} \times \sqrt{5})$R27°–Yb/Al(001) is shown in Fig. 1a.

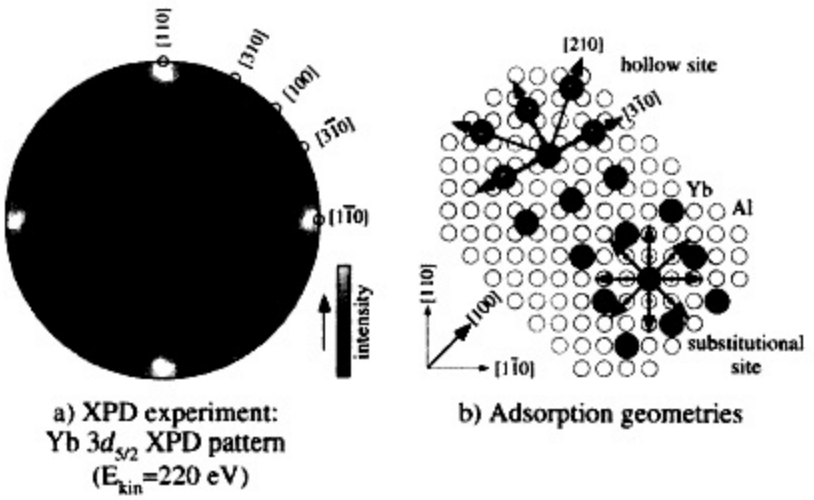


Fig. 1. (a) Experimental Yb $3d_{5/2}$ XPD pattern from $(\sqrt{5} \times \sqrt{5})$R27°–Yb/Al(001). The Yb $3d_{5/2}$ intensity has been transformed into a linear grey scale, while angles are projected stereographically: the center of the plot represents normal emission, and the outer circle corresponds to emission parallel to the surface. The mostly instrumental polar dependence of intensities has been removed by normalizing each azimuthal circle by its average intensity value. (b) Top view of Yb (full circles) on Al(001) adsorption geometries respecting the $(\sqrt{5} \times \sqrt{5})$R27° unit cell. For on-surface adsorption sites like the four-fold hollow site depicted in the upper part, in-plane near-neighbor forward focusing is expected along the $\langle 3\bar{1}0 \rangle$- and $\langle 210 \rangle$-like directions (arrows), which is not observed in the experiment. The experimental pattern in (a) gives direct evidence for occupation of substitutional sites as depicted in the lower part of the figure.

The pattern has been azimuthally averaged exploiting the four-fold rotational symmetry of the system, and normalized with respect to the mean intensity for each polar emission angle. The pattern is shown in stereographic projection. The center of the plot corresponds to the surface normal, and the outer circle represents grazing emission along the surface. Four dominant intensity maxima can be seen at very grazing emission angles in the ⟨110⟩ azimuths. The absence of forward-focusing peaks in the ⟨310⟩ and ⟨3$\bar{1}$0⟩ directions of the nearest-neighbor Yb atoms directly rules out simple on-surface adsorption geometries such as the four-fold hollow site shown in the top part of Fig. 1b. For the substitutional adsorption geometry on the other hand, the four intensity maxima in the ⟨110⟩ directions can be explained by nearest-neighbor Al forward-focusing, as shown schematically in the lower part of Fig. 1b.

The Yb $3d_{5/2}$ photoelectron diffraction pattern gives strong and direct evidence for substitutional site occupation, and this geometry has therefore been used as a starting configuration for a detailed full dynamical LEED analysis. Beside the first three substrate interlayer spacings and the vertical position of the Yb adsorbate, the lateral coordinates of the Al atoms within the first two layers and vertical relaxations within the first three layers have been refined in this analysis. Also, the Debye temperatures of the first-layer Al atoms and the Yb atoms were optimized, as well as the real part of the inner potential; the Debye temperature of the bulk Al atoms was kept fixed at its bulk value of 356 K. The optimum geometry with a corresponding Pendry $R$ factor of 0.28 is shown in Fig. 2, and a comparison of experimental and calculated $I$–$E$ spectra is given in Fig. 3. In the best-fit geometry, the Yb atoms are located $0.37 \pm 0.04$ Å above the top substrate layer, which is strongly reconstructed. The Al atoms are laterally displaced by 0.5 Å from their bulk positions, leading to a quasi-eight-fold coordination of Yb in the first layer. The nearest and next-nearest neighbor distances between Yb and Al in the first layer take values of $3.37 \pm 0.10$ and $3.51 \pm 0.10$ Å, respectively. Compared with the Al bulk value of 2.025 Å, the top-layer spacing of $2.22 \pm 0.04$ Å is strongly expanded by 10%. This expansion and the large vibrational amplitudes of

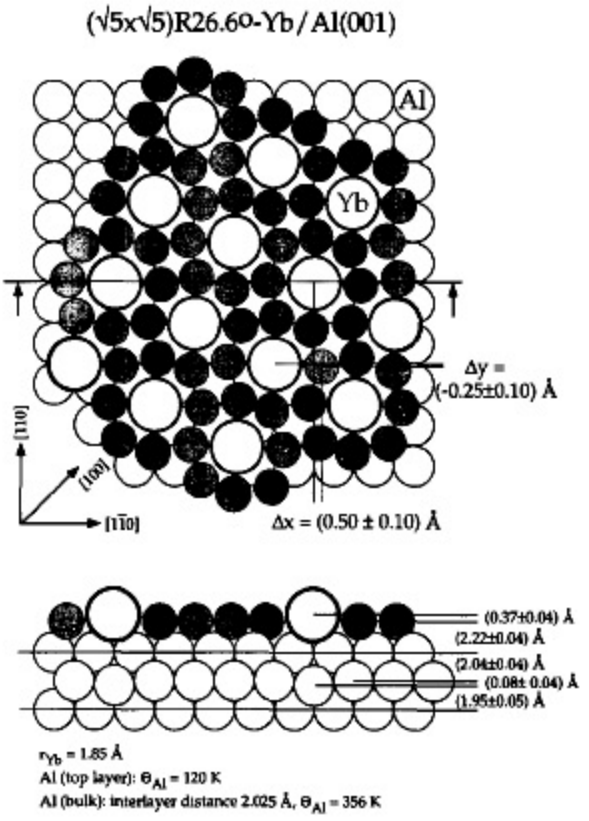


Fig. 2. Structural model of $(\sqrt{5} \times \sqrt{5})$R27°–Yb/Al(001) as determined by LEED. The best-fit parameter values are indicated.

the top-layer Al atoms corresponding to a Debye temperature of only 120 K ($\Theta_D$(bulk) = 356 K) give evidence for a substantial weakening of the bonding between the top substrate layer and the bulk. From the nearest-neighbor Yb–Al distance (second-layer Al atoms) of $3.29 \pm 0.05$ Å, an Yb hard-sphere radius of $1.86 \pm 0.05$ Å can be derived. A comparison with the values for metallic divalent Yb of 1.94 Å [21] and for trivalent Yb of 1.74 Å [21] suggests that the Yb atoms are in the divalent $4f^{14}$ state, and that therefore no hybridization of the 4f electrons with conduction electrons takes place in the $\sqrt{5}$ structure. This is confirmed by recent ultraviolet photoelectron spectroscopy data [22], and agrees well with findings on the homogeneous mixed-valent $YbAl_2$ and $YbAl_3$ intermetallic compounds, where the surface Yb atoms are also found in the divalent state [8,9].

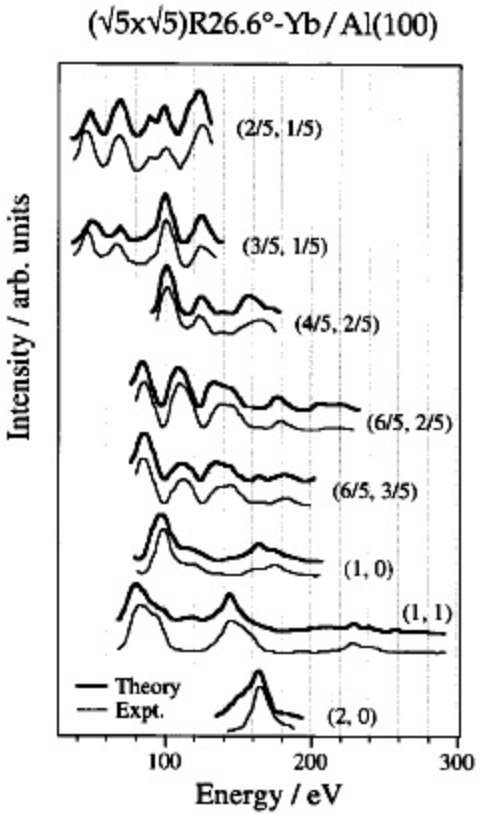


Fig. 3. Comparison of the experimental and calculated best-fit $I$–$E$ spectra for $(\sqrt{5}\times\sqrt{5})$R27°–Yb/Al(001) ($R_P = 0.28$). Beam $hk$ indices are indicated in the figure.

### *3.2. Structural analysis by XPD: inadequacy of the Debye–Waller model*

Following the LEED study, a quantitative structural analysis based on the XPD data of Fig. 1a has been performed. Using SSC calculations and an $R$ factor analysis, the lateral coordinates of the first-layer Al atoms, the vertical position of the Yb atoms, the effective inner potential [14], the inelastic mean free path of the photoelectrons, and the first-layer Al Debye temperature have been optimized. Since the Yb 3d XPD pattern is not very sensitive to the interlayer spacing between the composite Yb–Al layer and the first bulk Al layer, this parameter was kept fixed at the value of 2.22 Å determined by LEED. In agreement with the results from the LEED analysis, the top-layer Al atoms are found to be laterally displaced from their bulk positions by $\Delta x = 0.5 \pm 0.1$ Å [23] and $\Delta y = -0.15 \pm 0.1$ Å (Fig. 2). Large vibrational amplitudes corresponding to a Debye temperature of 100 K are found for this strongly reconstructed first substrate layer. However, the vertical position of the Yb atoms is found to be significantly different from that determined by LEED: whereas LEED determines a Yb–Al near-neighbour layer spacing of $0.37 \pm 0.04$ Å, the optimum value as derived by XPD is $0.1 \pm 0.1$ Å. In the following, we will show that by introducing a more appropriate description of vibrational effects in the SSC calculations, this discrepancy regarding the vertical position of the Yb atoms is lifted.

The result of an XPD-SSC calculation for the adsorption geometry derived by LEED (Fig. 2) is shown in Fig. 4. With the vertical Yb position of 0.37 Å, the Yb–Al forward-focusing directions point towards the bulk, and the calculated XPD pattern therefore contains only weak features from Yb–Al scattering. The dominant contribution to the diffraction pattern arises from intralayer Yb–Yb forward focusing along the ⟨310⟩-like directions (Fig. 4a). In the calculation where the two domains rotated by ±26.6° are considered (Fig. 4b), slightly enhanced intensity appears along the ⟨110⟩ directions due to the superposition of the first-order interference fringes around the ⟨310⟩ and ⟨3$\bar{1}$0⟩ Yb–Yb forward-focusing directions. The Yb–Yb forward-focusing maxima along these ⟨310⟩ and ⟨3$\bar{1}$0⟩ directions, however, still dominate the diffraction pattern, which is not the case in the experimental diffraction pattern of Fig. 1a.

As discussed above and shown schematically in Fig. 5a, in a static picture, the Al atoms located 0.37 Å below the Yb emitters contribute only little to the intensity enhancement at grazing emission angles along the ⟨110⟩ directions. For a part of the top-layer Al atoms, however, the vertical Yb–Al distance is considerably smaller than 0.37 Å due to their broad thermal distribution around the equilibrium position. The top-layer Al Debye temperature of 120 K as determined by LEED is connected with a room-temperature root mean square (RMS) displacement of 0.34 Å, which means that on average a significant fraction of first-layer Al atoms is located only slightly below or even above the Yb emitters. It can be expected that these Al atoms give rise to some forward-focusing

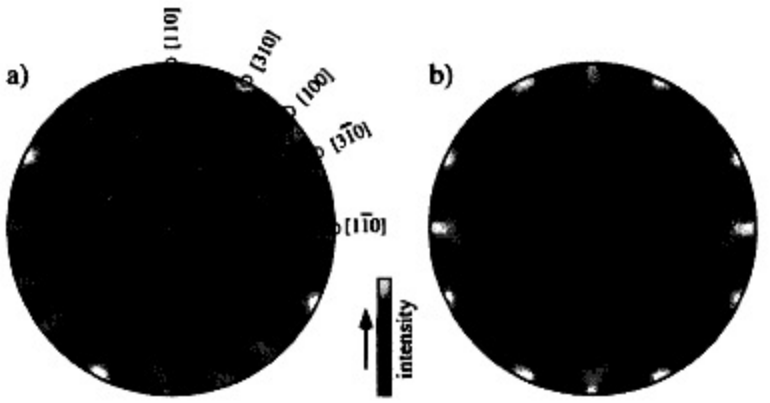


Fig. 4. XPD-SSC calculation for the best-fit geometry as determined by LEED and depicted in Fig. 2. (a) Calculation for one domain of the $(\sqrt{5}\times\sqrt{5})$R27° structure. The corresponding arrangement of atoms in the first layer is indicated. The diffraction pattern is dominated by features from intralayer Yb–Yb scattering. (b) Calculation considering both domains of the $(\sqrt{5}\times\sqrt{5})$R27° structure. No agreement with the experimental pattern (Fig. 1a) is obtained.

intensity enhancement along the ⟨110⟩ direction, as illustrated in Fig. 5b. As evidenced by the calculations described above, this effect cannot be observed when temperature effects are treated within the Debye–Waller model. An alternative way of considering the thermal distribution of the Al scatterers is given by the concept of split positions, as already used in LEED theory [24] and previously used in XPD to describe the effects of rotational vibrations of adsorbed CO molecules [25]. The basic idea is illustrated in Fig. 5c: first, the intensity is calculated for several vertical positions of the top-layer Al atoms. Then, these intensities are summed up, weighted with the occupation probability of the corresponding Al positions which follows a Gaussian distribution.

In contrast to this procedure, in LEED an amplitude mixing over the split positions is performed. This is necessary because the LEED electrons are scattered coherently from all atoms within the transfer width of the electron beam. In XPD, however, a mixing of the intensities is appropriate since most of the scattering paths contributing to the XPD pattern contain only one or a few scatterers; note that each photoelectron contributes incoherently to the diffraction pattern.

In order to compare the concept of split positions with the Debye–Waller model, we have performed SSC calculations for an Yb–Al dimer where the Al atom is located 0.37 Å below the Yb emitter, with an Yb–Al bond distance of 3.4 Å (Fig. 6a). For one calculation, vibrational effects have been considered by a Debye–Waller factor which was calculated with a one-dimensional Al RMS displacement of 0.23 Å, corresponding to a Debye temperature of 100 K. For a second calculation, the concept of split positions has been applied. A Gaussian distribution with the same RMS deviation of 0.23 Å has been taken as the envelope for the split positions. For seven discrete vertical positions of the Al scatterer, the intensity distributions have been calculated and averaged according to the Gaussian occupation probability. As a reference, the scattering from an Al atom with the bulk vibrational amplitude (one-dimensional RMS displacement 0.065 Å, $\Theta_D$(bulk) = 356 K) has also been calculated within the Debye–Waller model. As illustrated in Fig. 6b, the split positions lead to an intensity enhancement at grazing emission angles, whereas the intensity is even suppressed by the Debye–Waller factor. As a consequence of considering thermal vibrations by the concept of split positions instead of using a Debye–Waller factor, intensity otherwise scattered towards the bulk reappears on the upper hemisphere.

### *3.3. Structural analysis by XPD including the concept of split positions*

In order to verify whether the disagreement between XPD and LEED in the vertical position

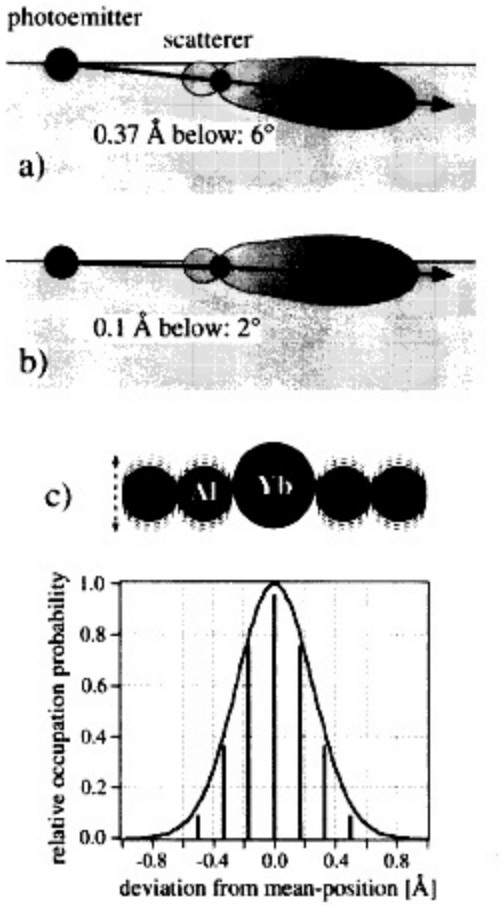


Fig. 5. (a) and (b): photoelectron scattering from a nearest-neighbor Al atom. The intensity scattered from the Al atom as calculated in a plane-wave approximation is shown as a function of scattering angle. (a) Yb–Al scattering situation for the geometry as determined by LEED. The Yb–Al forward-focusing direction points deeply into the bulk, and only little intensity is detected at grazing emission angles above the surface. (b) Yb–Al scattering situation for an Al atom located 0.1 Å below the Yb emitter. A significant intensity enhancement is observed along the surface. (c) Schematic illustration of the concept of split positions. The thermal vibrations of the Al atoms are considered by calculating the diffracted intensities for seven so-called "split positions", which are then summed up, weighted with the occupation probabilities of the corresponding Al positions.

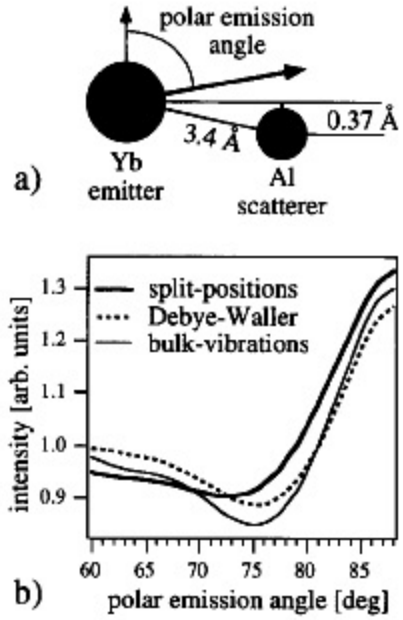


Fig. 6. (a) Schematic illustration of the scattering geometry corresponding to the adsorption model determined by LEED. The Al scatterer is located 0.37 Å below the Yb emitter with an Yb–Al bond length of 3.4 Å. (b) Calculated photoelectron intensity as a function of polar emission angle for the geometry depicted in (a). Thermal vibrations of the Al scatterer have been considered within the framework of the Debye–Waller model, and alternatively within the concept of split positions introduced above. A one-dimensional RMS displacement of 0.23 Å, corresponding to a Debye temperature of 100 K, has been used for the two calculations. For comparison, an additional calculation with the bulk Debye temperature of 356 K is shown. In the calculation with the split positions, an intensity enhancement at grazing emission angles is observed, whereas this intensity is even supressed in the calculation with the traditional Debye–Waller factor.

of the Yb atoms is indeed due to an inadequate description of the thermal vibrations of the top-layer Al atoms by the Debye–Waller factor, we have repeated the structural analysis of the XPD data including the concept of split positions as described above. The thermal vibrations of the top-layer Al atoms have been separated in vibrations perpendicular and parallel to the surface. The perpendicular vibrations have been accounted for by seven split positions, whereas the parallel vibrations have been taken into account within the framework of the Debye–Waller model. In this way, anisotropic vibrations can be described as well. The photoelectron diffraction intensities have been calculated for seven discrete positions of the entire top Al layer, consistent with correlated perpendicular vibrations of the top-layer Al atoms within a range determined by the inelastic mean-free path of the photoelectrons [26]. The seven

diffraction patterns have then been averaged according to the occupation probability of the Al atoms in the respective split position. A systematic multiparameter search has been performed. The structural parameters, the RMS displacements of the top-layer Al atoms perpendicular and parallel to the surface, as well as the "effective" inner potential $V_0$ (responsible for the refraction at the surface potential barrier [14,26]), and the electron inelastic mean-free path $\Lambda_e$ [26] have all been varied in the calculations.

The $R$-factor curves for the structural parameters after optimization of all the other parameters are given in Figs. 7b and 7d. As might have been expected, the split positions cause the $R$-factor minimum to shift from 0.1 Å to higher vertical Yb positions (Fig. 7d). The minimum value of the $R$ factor becomes lower upon this shift, which gives further evidence that the concept of split positions delivers a more appropriate description of vibrational effects in adsorbate XPD than the widely used Debye–Waller factor. For the optimum value of $0.25 \pm 0.05$ Å for the RMS displacement of the top-layer Al atoms perpendicular to the surface, the minimum in the $R_{MP}(z_{Yb})$ $R$-factor curve is found at a vertical Yb position of $0.35 \pm 0.1$ Å. This is in excellent agreement with the value of $0.37 \pm 0.04$ Å determined by LEED (Fig. 7c). Good agreement between the results from XPD and LEED is also obtained in the lateral displacements of the Al atoms within the strongly reconstructed top substrate layer. The $R$-factor contour plots for these displacements $\Delta x$ and $\Delta y$ resulting from the LEED and XPD analyses are given in Figs. 7a and 7c, respectively. Optimum values of $\Delta x = 0.5 \pm 0.1$ Å and $\Delta y = -0.15 \pm 0.1$ Å are obtained from the XPD analysis, whereas the values determined by LEED are $0.5 \pm 0.1$ and $-0.25 \pm 0.1$ Å, respectively. A compilation of the optimized parameters as determined by XPD and LEED is given in Table 1. Given the complexity of the $(\sqrt{5} \times \sqrt{5})$R27°–Yb/Al(001) structure, the level of agreement between the results derived from the two methods is very satisfactory.

An interesting feature of the present system is the observation of large RMS deviations for the Al atoms in the reconstructed first substrate layer. In order to determine whether these RMS deviations are due to static disorder or thermal vibrations, additional experiments would be necessary (for example, temperature-dependent LEED $I$–$E$ measurements). We believe, however, that the large RMS deviations are due to thermal vibrations rather than to static disorder, since static disorder, i.e. a vertical buckling of Al in the first layer, would lead to a breaking of the four-fold symmetry of the substitutional geometry in the $\sqrt{5}$ structure.

Enhanced surface vibrations of Al atoms have recently also been reported for the Rb/Al(111) system at low temperatures, where Rb occupies the on-top site [27]. A comparison of Yb/Al(001) with the $(\sqrt{3} \times \sqrt{3})$R30°–Rb/Al(111) system at room temperature, where the Rb atoms occupy substitutional sites [27], reveals, however, some differences. For Rb/Al(111), the enhanced first-layer Al vibrations have only been found for Rb adsorption in the metastable on-top geometry at low temperatures, whereas no vibrational "anomaly" has been found for the substitutional geometry in the room-temperature system. Another notably different behaviour is observed with respect to the outermost substrate layer spacing. In the case of Rb/Al(111), Rb substitutional site occupation leads to a contraction of the outermost substrate layer spacing from 2.33 to 2.27 Å, whereas a strong expansion is induced by Yb adsorption on Al(001). One can now speculate that these differences between the Rb/Al(111) and the Yb/Al(001) system are due to geometrical reasons: in the Yb/Al(001) substitutional geometry, the remaining first-layer Al atoms are shifted away from their equilibrium positions, thus allowing the Yb atoms to come closer to the surface. The outermost layer itself is then strongly laterally compressed, as evidenced by a comparison of the Al hard-sphere radii of 1.2 Å (top layer) and 1.43 Å (bulk). The lateral compression of the first layer goes along with a vertical expansion of the first interlayer spacing, which may be traced back to the tendency to keep the local Al density in the first layers at least roughly constant. As evidenced by the large vibrational amplitudes, this expansion is connected with a weakening of the bonding between the first-layer Al atoms and the bulk. In contrast to the $\sqrt{5}$ phase of Yb/Al(001), for the substitutional geometry of $(\sqrt{3} \times \sqrt{3})$R30°–Rb/Al(111), lateral shifts of top-

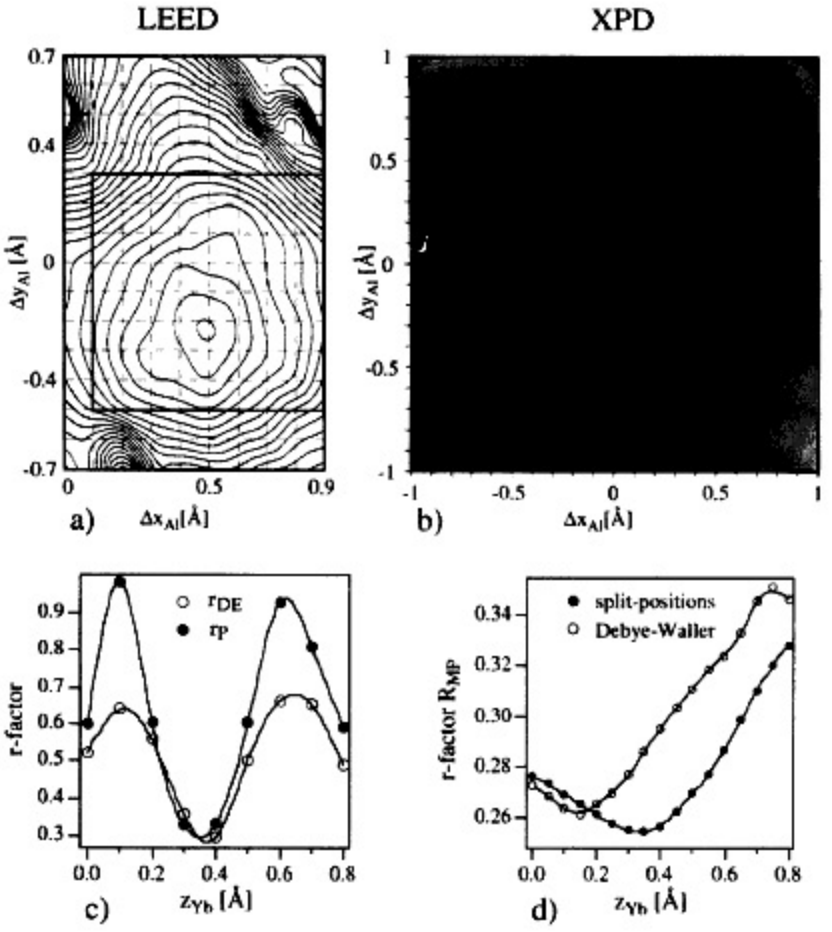


Fig. 7. (a) LEED and (b) XPD $R$-factor contour plots as a function of lateral displacements $\Delta x$ and $\Delta y$ of the top substrate layer Al atoms (Fig. 2). Note the different scales: The squares in the two plots indicate identical areas in parameter space. (c), (d): LEED (c) and XPD (d) $R$ factors as a function of vertical Yb position.

layer Al atoms are not compatible with the symmetry of the structure, so that the above considerations do not hold for this system.

### *3.4. Identification of subsurface Yb atoms by XPD*

Due to the absence of pronounced forward-focusing peaks at non-grazing emission angles in an adsorbate system, XPD is extremely sensitive to the presence of adsorbate-atom subsurface species. Photoelectrons emitted from atoms which have diffused into the second or deeper substrate layers are scattered from the substrate atoms on their way to the surface, and the respective scattering directions are reflected as intensity enhancements in the diffraction pattern. Due to this extreme sensitivity of XPD to buried emitters, as little as 1% of a monolayer of subsurface atoms can be detected [4].

Close inspection of the experimental Yb $3d_{5/2}$ diffraction pattern (Fig. 1a) indeed reveals the presence of this kind of intensity enhancement. The diffraction pattern shows intensity enhancements at about a 45° polar emission angle in the four $\langle 100\rangle$-like azimuths ($\langle 0\bar{1}1\rangle$ directions), which are not reproduced by the SSC calculation (not shown) for the best-fit geometry discussed above. The missing element in the calculation might therefore be the presence of a few percent of a monolayer of Yb atoms which have diffused into deeper Al substrate

Table 1
Optimum structural parameters of $(\sqrt{5}\times\sqrt{5})$R26.6°–Yb/Al(001) as determined by LEED and XPD: lateral displacements $\Delta x$ and $\Delta y$ of the residual Al atoms within the strongly reconstructed top substrate layer (Fig. 2), vertical position $z_{Yb}$ of the Yb atoms with respect to the top substrate layer, top substrate layer spacing $z_{12}$ (first-layer Al to second-layer Al), second substrate layer spacing $z_{23}$ (second-layer Al to third-layer Al), third substrate layer spacing $z_{34}$ (third-layer Al to fourth-layer Al), buckling of third-layer Al atoms $\Delta z_3$, first-layer Al rms displacements perpendicular ($\sqrt{\langle u^2\rangle}^{\perp}_{(Al\ 1st)}$) and parallel ($\sqrt{\langle u^2\rangle}_{(Al\ 1st)}$) to the surface, and Debye temperature of the top-layer Al atoms $\Theta_{D(Al\ 1st)}$

| Parameter | LEED | XPD |
|---|---|---|
| $\Delta x$ (Å) | 0.50±0.1 | 0.50±0.1 |
| $\Delta y$ (Å) | −0.25±0.1 | −0.15±0.1 |
| $z_{Yb}$ (Å) | 0.37±0.04 | 0.35±0.1 |
| $z_{12}$ (Å) | 2.22±0.04 | — |
| $z_{23}$ (Å) | 2.04±0.04 | — |
| $z_{34}$ (Å) | 1.95±0.05 | — |
| $\Delta z_3$ (Å) | 0.08±0.04 | — |
| $\sqrt{\langle u^2\rangle}^{\perp}_{Al\ 1st}$ (Å) | — | 0.25±0.05 |
| $\sqrt{\langle u^2\rangle}_{(Al\ 1st)}$ (Å) | — | 0.25±0.1 |
| $\Theta_{D(Al\ 1st)}$(K) | 120 | (114) |

layers. In fact, the intensity enhancements along these $\langle 0\bar{1}1\rangle$ directions can easily be explained by the coexistence of smaller surface regions where some Yb atoms occupy second-layer Al sites. The situation is depicted schematically in Fig. 8a: photoelectrons emitted from the subsurface Yb atoms are forward focused by their nearest-neighbor Al surface atoms, which gives rise to the observed intensity enhancement along the $\langle 0\bar{1}1\rangle$ directions.

The diffusion of Yb atoms into deeper Al layers is not that unexpected. It was shown as early as 1980 by Tibbetts and Egelhoff [10] that interdiffusion starts slightly above room temperature, and that it becomes substantial at temperatures above 100°C. For Yb on Al(110), it has been shown by Onsgaard et al. [28] that slow interdiffusion already takes place at room temperature, and that a strongly enhanced diffusion occurs when the temperature is increased to 300°C. Furthermore, it is well known that Yb and Al form intermetallic compounds, namely $YbAl_2$ with the cubic $MgCu_2$ structure, and $YbAl_3$ with the cubic $Cu_3Au$ structure [7]. From the fact that Yb is in a mixed-valent state in both of these intermetallic compounds [7] arises the interesting possibility to strengthen the arguments for the presence of second-layer Yb atoms given above. In Yb 3d photoemission, the strong Coulomb interaction between the 3d core hole and the 4f shell splits the core-level final states for different 4f occupancies. It has been shown by Degiorgi et al. [29] for YbP

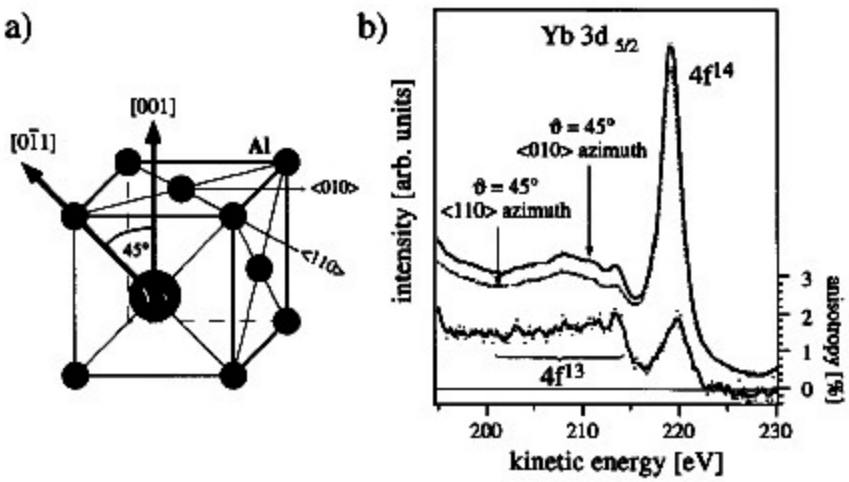


Fig. 8. Identification of subsurface Yb atoms by XPD. (a) Scattering geometry for a Yb atom in a second-layer Al site. Forward focusing along nearest-neighbor directions is expected to give rise to enhanced intensity along the $\langle 0\bar{1}1\rangle$ directions. (b) Angle-resolved Yb $3d_{5/2}$ photoelectron spectra measured at 45° polar emission angle along a $\langle 0\bar{1}1\rangle$-type direction ($\langle 010\rangle$ azimuth) and halfway between two $\langle 0\bar{1}1\rangle$-type directions ($\langle 110\rangle$ azimuth). The anisotropy (see text) of the two spectra is given in the lower part of the figure. The dots are raw data, and the lines have been obtained by a smoothing operation.

that the Yb $4f^{13}$ ground state gives rise to spectral weight in the 3d final states which is well separated from the 3d peaks corresponding to the divalent $4f^{14}$ ground state. Under the assumption that the second-layer Yb atoms which give rise to the intensity enhancement along the $\langle 0\bar{1}1\rangle$ directions (Figs. 1 and 8a) are in a mixed-valent $4f^{14-\delta}$ state, enhanced $3d^94f^{13}$ spectral weight should also be observed along these $\langle 0\bar{1}1\rangle$ directions. The appearance of enhanced $3d^94f^{14}$ *and* $3d^94f^{13}$ intensity along the $\langle 0\bar{1}1\rangle$ directions would therefore be a strong indication for mixed valent Yb in second-layer Al sites.

The angle-resolved Yb $3d_{5/2}$ photoemission spectra measured at a polar emission angle of 45° along a $\langle 0\bar{1}1\rangle$-type direction and halfway between two $\langle 0\bar{1}1\rangle$-type directions are shown in Fig. 8b. In the lower part of Fig. 8b, the anisotropy of the two spectra is given, which is defined as the ratio of the difference and the sum of the two spectra. The intensity enhancement along the $\langle 0\bar{1}1\rangle$ directions observed in the diffraction pattern of Fig. 1 is clearly reflected in the upper spectrum of Fig. 8b as increased intensity of the main $4f^{14}$ line ($E_{kin}$ = 220 eV). The broad shoulders at lower kinetic energy have been interpreted as a superposition of electron energy-loss peaks and possible $3d^94f^{13}$ spectral weight [30,31], which makes a straightforward interpretation difficult. However, the anisotropy curve in the lower part of Fig. 8b clearly reveals the typical $3d^94f^{13}$ multiplet structure as, is found, for example, in the Yb hydrides [32] or the Yb pnictides YbN, YbP and YbAs [33]. The fact that this anisotropy is positive means that an increased intensity of Yb 3d photoelectrons emitted from Yb atoms in the trivalent $4f^{13}$ ground state is observed along the $\langle 0\bar{1}1\rangle$ directions, supporting the above assumption of mixed-valent second-layer Yb atoms. The photoelectrons emitted from these subsurface Yb atoms are forward focused by the surface Al atoms, and therefore give rise to the observed intensity enhancement along the $\langle 0\bar{1}1\rangle$ directions.

We would like to mention that it is difficult to detect the coexistence of smallest surface areas containing a few per cent of a monolayer of subsurface Yb atoms by LEED. Since these areas do not have $\sqrt{5}$ periodicity, they do not affect the fractional-order beams. They can, however, influence the integer-order *I–E* curves. A closer inspection of the *R* factors and of the measured and calculated *I–E* curves (Fig. 3) indeed reveals that the agreement of the integer-order beams is not as good as for the fractional-order beams, which may be due to the coexistence of a second phase without $\sqrt{5}$ periodicity.

Neglecting domain-boundary effects, the coexistence of different domains is reflected in an XPD pattern as an incoherent superposition of the diffraction patterns corresponding to the individual domains. In order to include the presence of a few percent of subsurface Yb atoms in our calculations, we have performed a SSC calculation for an Yb emitter located at a second-layer Al site. The undisturbed Al surface structure has been assumed, neglecting possible relaxation effects due to the Yb subsurface impurity. The diffraction intensities calculated in this way have then been added to the diffraction pattern calculated for the best-fit $(\sqrt{5}\times\sqrt{5})$R26.6°–Yb/Al(001) geometry. Best agreement with experiment is achieved for a superposition of the calculation for the subsurface Yb emitter with 15% weight, and for the $(\sqrt{5}\times\sqrt{5})$R26.6°–Yb/Al (001) geometry with 85% weight. This corresponds to a surface composition of 0.17 ML Yb atoms in the $\sqrt{5}$ structure and of 0.03 ML Yb atoms in second-layer Al sites in unreconstructed surfaces patches. The resulting SSC calculation is compared in Fig. 9 to the experimental Yb $3d_{5/2}$ XPD pattern.

## 4. Conclusions

The surface structure of $(\sqrt{5}\times\sqrt{5})$R27°–Yb/Al (001) has been determined by means of LEED and XPD. Quantitative agreement between the results from the two techniques has been obtained. The Yb atoms are found to be located in substitutional sites within a strongly reconstructed Al surface layer. These first-layer Al atoms are displaced by more than 0.5 Å from their equilibrium position, in a way that results in a quasi-twelve-fold Al coordination for the Yb atoms. A strong expansion of the outermost layer spacing and large vibrational amplitudes of the top-layer Al atoms are

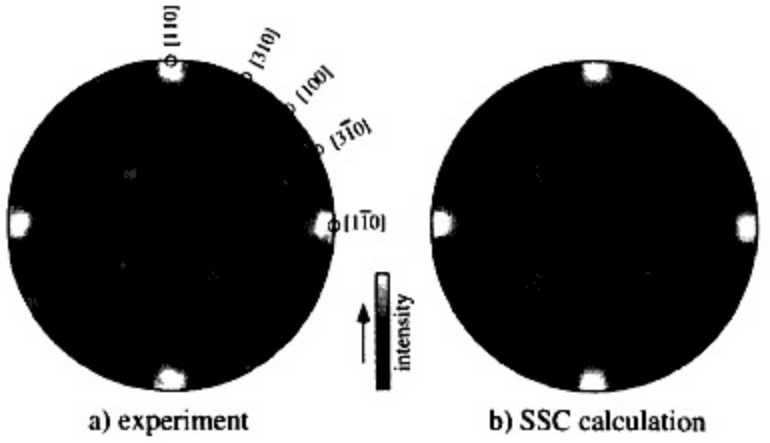


Fig. 9. (a) Experimental Yb $3d_{5/2}$ XPD pattern of Fig. 1a compared with the SSC calculation (b) for 0.17 ML Yb in the best-fit $(\sqrt{5} \times \sqrt{5})R27°$ geometry and 0.03 ML Yb in second-layer Al sites.

found, giving evidence for a substantial adsorbate-induced weakening of the bonding between the top substrate layer and the bulk.

Due to the extreme sensitivity of XPD to buried emitters, the presence of Yb atoms diffused into the second substrate layer has been identified. It has been shown that small unreconstructed surface patches with Yb atoms in second-layer Al sites coexiste with the long-range $(\sqrt{5} \times \sqrt{5})R27°$ reconstruction. The combination of XPD and LEED has proved to be very powerful: very direct structure information is delivered by XPD, which can then be used as a starting point for a very accurate structure determination by LEED. Furthermore, as LEED probes only that part of the surface which shows long-range order, XPD can provide additional information on surface patches without long-range order.

An initial discrepancy in the structural parameters as determined from LEED and XPD has been shown to be due to an inappropriate consideration of thermal vibrations in the modeling of the XPD data. The introduction of the concept of split positions has been shown to remove this discrepancy. In quantitative XPD from adsorbate atoms, the traditional Debye–Waller model must therefore be applied with care wherever thermal vibrations are expected to be important.

## Acknowledgements

We thank T. Greber for many invaluable discussions. One of the authors (R.F.) gratefully acknowledges the Fritz-Haber Institute for kind hospitality. Skilful technical assistance was provided by E. Mooser, O. Raetzo, F. Bourqui and H. Tschopp. This project has been supported by the Fonds National Suisse pour la Récherche Scientifique.

## References

[1] J.B. Pendry, Low Energy Electron Diffraction (Academic Press, London, 1974).
[2] C.S. Fadley, in: Progress in Surface Science, Vol. 16, Ed. S.G. Davison (Pergamon, New York, 1984) p. 275; C.S. Fadley, in: Synchrotron Radiation Research: Advances in Surface Science, Ed. R.Z. Bachrach (Plenum, New York, 1990) ch. 11.
[3] R. Fasel, P. Aebi, L. Schlapbach and J. Osterwalder, Phys. Rev. B 52 (1995) R2313.
[4] J. Osterwalder et al., Surf. Sci. 331–333 (1995) 1002.
[5] R. Fasel and J. Osterwalder, Surf. Rev. Lett. 2 (1995) 359.
[6] R. Fasel, P. Aebi, J. Osterwalder and L. Schlapbach, Surf. Sci. 331–333 (1995) 80.
[7] E.E. Havinga, K.H.J. Buschow and H.J. van Daal, Solid State Commun. 13 (1973) 621.
[8] G. Kaindl et al., Solid State Commun. 41 (1982) 157.
[9] S.-J. Oh et al., Phys. Rev. B 37 (1988) 2861.

[10] G.G. Tibbetts and W.F. Egelhoff, Jr., J. Vac. Sci. Technol. 17 (1) (1980) 458.
[11] D.J. Friedman and C.S. Fadley, J. Electron Spectrosc. Relat. Phenom. 51 (1990) 689.
[12] J.J. Rehr, R.C. Albers, C.R. Natoli and E.A. Stern, Phys. Rev. B 34 (1986) 4350; J. Mustre de Leon, J.J. Rehr, C.R. Natoli, C.S. Fadley and J. Osterwalder, Phys. Rev. B 39 (1989) 5632.
[13] J.J. Yeh and I. Lindau, At. Data Nucl. Data Tables 32 (1985) 1.
[14] R. Fasel et al., Phys. Rev. B 50 (1994) 14516.
[15] W. Moritz, J. Phys. C 17 (1983) 353.
[16] R. Feder and W. Moritz, Surf. Sci. 77 (1978) 505.
[17] G. Kleinle, W. Moritz, D.L. Adams and G. Ertl, Surf. Sci. 219 (1989) L637.
[18] J.B. Pendry, J. Phys. C 13 (1980) 937.
[19] G. Kleinle, W. Moritz and G. Ertl, Surf. Sci. 238 (1990) 119.
[20] M. Gierer, H. Over and W. Moritz, unpublished.
[21] B.J. Beaudry and K.A. Gschneidner, in: Handbook on the Physics and chemistry of Rare Earths, Volume 1: Metals, Eds. K.A. Gschneidner and L. Eyring (North-Holland, Amsterdam, 1978).
[22] R. Fasel, P. Aebi, T. Greber, J. Osterwalder and L. Schlapbach, Surf. Rev. Lett., in press.
[23] So far, no rigorous theory for error estimation has been developed for the multipole $R$ factor $R_{MP}$ used in the present XPD study. The errors indicated for the structural parameters determined from the XPD data are estimates.
[24] H. Over, W. Moritz and G. Ertl, Phys. Rev. Lett. 70 (1993) 315.
[25] P.J. Orders, S. Kono, C.S. Fadley, R. Trehan and J.T. Lloyd, Surf. Sci. 119 (1982) 371.
[26] The inelastic mean-free path of the Yb $3d_{5/2}$ photoelectrons at 220 eV kinetic energy turns out to be of the order of 2 Å. The optimum value of the effective inner potential is found to be $V_0 = 3$ eV. In all the calculations shown, these optimum values have been used. For a discussion of the reasons underlying these relatively low values, see Ref. [14].
[27] M.M. Nielsen, J. Burchhardt, D.L. Adams, E. Lundgren and J.N. Andersen, Phys. Rev. Lett. 72 (1994) 3370.
[28] J. Onsgaard, I. Chorkendorff, O. Ellegaard and O. Sørensen, Surf. Sci. 138 (1984) 148.
[29] L. Degiorgi et al., Europhys. Lett. 4 (1987) 755.
[30] R. Fasel, Diploma Thesis, Université de Fribourg, 1991.
[31] T. Greber, J. Osterwalder and L. Schlapbach, Phys. Rev. B 40 (1989) 9948.
[32] S. Büchler, L. Schlapbach, R. Monnier and L. Degiorgi, J. Phys. 48 C9 (1987) 947.
[33] T. Greber et al., J. Phys. 48 C9 (1987) 943.